Published in final edited form as:

*J Biomater Appl*. 2013 July ; 28(1): 100–111. doi:10.1177/0885328212437883.

# A dual-modal magnetic nanoparticle probe for preoperative and intraoperative mapping of sentinel lymph nodes by magnetic resonance and near infrared fluorescence imaging

**Zhengyang Zhou**[1,2], **Hongwei Chen**[1,3], **Malgorzata Lipowska**[1], **Liya Wang**[1,3], **Qiqi Yu**[1,3], **Xiaofeng Yang**[1,3], **Diana Tiwari**[1,3], **Lily Yang**[1,4], and **Hui Mao**[1,3]

[1]Department of Radiology and Imaging Sciences, Emory University School of Medicine, Atlanta, GA, USA

[2]Department of Radiology, Drum Tower Hospital, College of Medicine, Nanjing University, Nanjing, China

[3]Center for Systems Imaging, Emory University School of Medicine, Atlanta, GA, USA

[4]Department of Surgery, Emory University School of Medicine, Atlanta, GA, USA

## Abstract

The ability to reliably detect sentinel lymph nodes for sentinel lymph node biopsy and lymphadenectomy is important in clinical management of patients with metastatic cancers. However, the traditional sentinel lymph node mapping with visible dyes is limited by the penetration depth of light and fast clearance of the dyes. On the other hand, sentinel lymph node mapping with radionucleotide technique has intrinsically low spatial resolution and does not provide anatomic details in the sentinel lymph node mapping procedure. This work reports the development of a dual modality imaging probe with magnetic resonance and near infrared imaging capabilities for sentinel lymph node mapping using magnetic iron oxide nanoparticles (10 nm core size) conjugated with a near infrared molecule with emission at 830 nm. Accumulation of magnetic iron oxide nanoparticles in sentinel lymph nodes leads to strong $T_2$ weighted magnetic resonance imaging contrast that can be potentially used for preoperative localization of sentinel lymph nodes, while conjugated near infrared molecules provide optical imaging tracking of lymph nodes with a high signal to background ratio. The new magnetic nanoparticle based dual imaging probe exhibits a significant longer lymph node retention time. Near infrared signals from nanoparticle conjugated near infrared dyes last up to 60 min in sentinel lymph node compared to that of 25 min for the free near infrared dyes in a mouse model. Furthermore, axillary lymph nodes, in addition to sentinel lymph nodes, can be also visualized with this probe, given its slow clearance and sufficient sensitivity. Therefore, this new dual modality imaging probe with the tissue penetration and sensitive detection of sentinel lymph nodes can be applied for preoperative survey of lymph nodes with magnetic resonance imaging and allows intraoperative sentinel lymph node mapping using near infrared optical devices.



Corresponding author: Hui Mao, Department of Radiology and Imaging Sciences, Emory University School of Medicine, 1364 Clifton Road, Atlanta, GA 30322, USA. hmao@emory.edu.

**Keywords**

Sentinel lymph node; metastasis; nanoparticles; near infrared; magnetic resonance imaging; optic imaging

## Introduction

Metastasis of cancer cells to lymph nodes is the one of the most important prognostic markers and a determinant predictor of recurrence and survival in cancer patients. Because sentinel lymph node (SLN) is the first lymph node to receive lymphatic drainage from a primary tumor, the ability to reliably detect SLNs and relevantly carry on SLN biopsy might avoid the unnecessary full lymphadenectomy.[1,2] Currently, SLN detection has been applied in the clinical management of many types of solid tumors, including melanoma, head and neck cancer, breast cancer, lung cancer, gastric cancer and colorectal cancer.[3–5] For example, metastatic breast cancer has distant organ involvement and is not operatable. Therefore, SLN mapping is used to prevent local and distant recurrence for breast cancers. Although traditional SLN imaging is performed with a color (e.g. Evans blue) dye or a radiolabeled tracer in the clinical practices, there are some significant disadvantages and limitations in these methods.[6,7] For example, organic dyes visible by the surgeon's naked eye do not have deep tissue penetration. They have poor tissue contrast and are difficult to detect deeper lymph nodes. Additionally, blue dye molecules can quickly spillover from SLNs to the subsequent distant lymph nodes, leading to a high rate of false-positive in detecting SLNs. On the other hand, radionucleotide technique has intrinsically low spatial resolution and does not provide anatomic details in the SLN mapping procedure. Furthermore, it exposes patients and health care personnel to ionizing radiation even though it is at the lowest dosage. The high activity from the radioactive tracer injected in the primary injection site can interfere with intraoperative detection of nearby nodes.[1,8]

To date, ultrasound, computed tomography, magnetic resonance imaging (MRI) and optical imaging have been investigated in the preoperative and intraoperative detection and mapping of SLNs.[3,9–15] With exquisite soft-tissue contrast and superb spatial resolution for anatomic details, MRI is ideal for MR lymphography with novel gadolinium (Gd)-based contrast agents, that is, mapping a set of lymph nodes preoperatively.[16] The development of molecular and targeted MRI contrast agents may enable detecting the lymph nodes with metastasis in order to identify the candidates need for SLN removal.[17] With the new generation of tracers, such as near infrared (NIR) dyes with improved tissue penetration by NIR imaging, optical imaging allows for intraoperatively localizing nodes with high sensitivity, good tissue penetration and real-time data acquisition. Both modalities are playing increasing roles in the clinical management of cancer patients for mapping of SLN. However, the use of a single imaging modality alone has practical limitations in accurate and comprehensive lymphatic mapping. Because of complicated setup and cost-effective concerns, it is difficult to use MRI for real-time visualization during the procedure, while optical imaging does not typically have three-dimensional (3D) tomography capability as light only penetrates tissues within 1–2 cm. Thus, it is conceivable that dual modality MR and optical fluorescence imaging will overcome the limitations in SLN mapping.

Previously, several studies have investigated MR-fluorescence imaging probes, using Gd-based MRI contrast agents linked with fluorescent and/or NIR dyes for dual-modal imaging mapping of SLN,[18–20] promoting the further development of this approach for improvement of the conventional SLN mapping. Herein, we report the development of a new class of dual modality MR and NIR imaging probe using biocompatible iron oxide nanoparticles (IONPs) conjugated with a NIR molecule with emission wavelength at 830nm for SLN mapping. The capability of MR and optical imaging of sentinel and axillary lymph nodes was investigated in a mouse model.

## Materials and methods

### Synthesis of NIR dye NIR830

The NIR830 dye (Figure 1), containing a succinimido carboxylate functional group as an aminoreactive group, was synthesized from IR-783 in two steps in a manner described before.[21] IR-783, 4-mercaptobenzoic acid (4-MBA), N,N′-disuccinimidyl carbonate (DSC) and other chemicals and solvents for the synthesis were purchased from Sigma-Aldrich (St. Louis, MO). Electrospray mass spectrometry (MS) was performed on a Finningan LTQ-FT instrument (Thermo Electron). Briefly, IR-783 was allowed to react with 4-MBA in anhydrous DMF overnight at room temperature under a nitrogen atmosphere with a molar ratio of IR-783: 4-MBA=1:3. NIR830-COOH (1), which precipitated from the reaction mixture upon addition of ethanol/ether (1:20), was separated, washed with ether and vacuum dried. NIR-830-NHS (2) was obtained by estrification of the carboxylic acid function in 1 with DSC in anhydrous DMF (NIR830-COOH: DSC=1:1.2). After the reaction mixture was stirred at room temperature for 24 h under a nitrogen atmosphere, ether was slowly added and the resulting crystalline precipitate of succinate ester 2 was filtered, washed with ether and vacuum dried. $\lambda_{max}$ (water)=791 nm, $\lambda_{em}$ (water)=810 nm. MS using probe electrosprayionization (PESI): m/z 940 (100%, $M^-$); high-resolution MS calculated for $C_{49}H_{54}N_3O_{10}S_3$: 940.29768, found: 940.29945. All the reactions are highly efficient and purification of all products 1 and 2 does not require chromatography.

### Preparation of magnetic IONPs

Hydrophobic iron oxide nanocrystals with a core size of 10nm were prepared by heating iron oxide powder and oleic acid in octadecene at 315°C.[22] The hydrophobic IONPs then were coated and stabilized with an antibiofouling diblock copolymer poly(ethylene oxide)-*block*-poly(γ-methacryloxypropyl tri-methoxysilane) (PEO-*b*-PγMPS) reported previously.[23,24] Briefly, the nanocrystals were mixed with the newly synthesized copolymer in anhydrous tetrahydrofuran (THF). After being aged for 4 days, the mixture was added drop-wise into water with gentle magnetic stirring. THF in the solution was removed by dialysis using deionized water. The IONP solution was then purified by using a magnetic separator (Frantz laboratory) to get rid of free polymers.

### Conjugation of NIR830-NHS dye to IONPs

IONPs were functionalized with amine groups on the nanoparticle surface as previously described.[23] NIR830-NHS then was conjugated on IONP with the procedure illustrated in Figure 2(a). Briefly, 1.0mL aqueous IONPs (1.0 mg iron [Fe]) with 10nm core size as shown

in transmission electron microscopy (Figure 2(b)) was added with 1.0 μL (3-aminopropyl) trimethoxysilane (APTMS) in 20 μL dimethyl sulfoxide (DMSO). The mixture was gently stirred at room temperature for 2 days. The resultant solution was purified through a PD-10 column (GE Healthcare). IONPs functionalized with amine groups were dissolved with sodium carbonate to form a 0.1M solution with a pH of 9. NIR830-NHS (0.4 mg) dissolved in 400 μL $H_2O$ was added to this solution immediately. The reaction for conjugating NIR830 to IONPs was carried out for 2 h at room temperature. The resultant IONP-NIR830 product was purified using Easysep® magnet for three times. The final Fe concentration (1.0 mg/mL Fe) was determined by spectrophotometry.[25] The concentration of NIR830 dye in IONP-NIR830 conjugates was estimated based on a concentration curve of the standard solution determined at its absorption at 791 nm. The zeta potential, average hydrodynamic diameters and size distributions of IONPs and composited IONP-NIR830 nanoparticles were measured using a dynamic light scattering (DLS) instrument (Malvern Zeta Sizer Nano S-90) equipped with a 22 mW He–Ne laser operating at λ=632.8 nm.

### MRI and NIR imaging contrast of IONP-NIR830

To investigate the MRI and NIR imaging properties of the IONP-NIR830 probe, the solution samples of IONP-NIR830 at different concentrations were placed in the optical and MRI compatible tubes and scanned on a 3 Tesla MRI scanner (Magneto Tim/Trio, Siemens Healthcare, German). Longitudinal and transverse relaxation times, $T_1$ and $T_2$, of the samples were measured using the methods reported previously.[26] Spectra and NIR image data of the samples were recorded on a multispectral spectroscopic imaging unit (Maestro, CRi Inc, Woburn, MA, USA).

### MRI and NIR imaging of lymph nodes in mice

Female nude mice ($N$=12, weight of 20–25 g, Charles River) were used in this study. Mice were acclimated for 2 weeks prior to use. An alfalfa-free rodent diet (Teklad 2918, Harlan Teklad) was used to reduce tissue autofluorescence. All experiments were performed under anesthesia using 2% isoflurane gas in oxygen.

During imaging, mice were maintained in the anesthetized state. Mice were randomly assigned to two experimental groups: one group ($N$=6) received free NIR830 dye, while the other group ($N$=6) received the IONP-NIR830 probe. Imaging tracers (25 μL) were administrated into the middle phalange of either fore footpad and/or into the middle digit of the hind footpad of each animal, allowing for tracers to be immediately delivered to the lymphatic systems.

NIR imaging of animals administrated with SLN tracers were obtained using the Mastro multispectral spectroscopic imager. In all cases, optical image data were acquired using an excitation 684–729nm band pass filter and an emission 745nm long pass filter, respectively. The tunable filter was automatically increased in 30nm increments from 770 to 860nm to obtain spectroscopic data. A digital camera was used to capture images at each wavelength using a constant exposure. The consecutive NIR images were recorded once prior to the administration of the contrast agent, as well as at 5, 15, 30, 45, 60, 90 and 120 min thereafter. The camera exposure time was 90 s for the animals in the group that received the

NIR830 dye and 120 s for the group injected with IONP-NIR830, given a lower extinction coefficient of IONP-NIR830.

Animal MRI experiments were carried out on the 3 Tesla MRI scanner using a wrist coil and $T_2$ weighted fast spin echo and gradient echo fast low angle shot (FLASH) sequences. Animals that received imaging probes were scanned before and 2 h after the injection of the probes. Scan parameters include: field of view (FOV) of 120mm by 50 mm, matrix of 320 by 320, slice thickness of 0.6mm with no gap, repetition time (TR) of 3600 ms and echo time (TE) of 80 ms.

### Confirmation of imaging of lymph nodes in mice by blue dye staining

To stain the lymphatic vessels and the lymph nodes, each mouse received a subcutaneous injection of a total of 5 μL of 1% Evans blue dye (Kanto Chemistry KK, Tokyo, Japan) at the same sites as the administration of the contrast agent after the completion of MRI and NIR imaging. Animals were then sacrificed by exsanguination 10 min later, and the skin was removed in the area where the NIR signal had been detected to permit direct visualization of the dye. The axillary, popliteal and external iliac nodes appeared blue-stained under bright light, and their localizations were compared to those of optical and MRI mapping. For histological examination, all of the blue-stained nodes were evaluated on hematoxylin/eosin-stained tissue sections.

### Image and data analysis

To determine the NIR signal changes in SLNs over the time, the signal intensity in the SLNs and background signal (autofluorescence of tissues) were measured in the regions of interest (ROIs) around the different SLN (axillary, popliteal and inguinal nodes) drawn on NIR images. The ROI size was adapted to encompass the entire lymph node. The ROIs were kept unchanged in size and position for all image sets obtained within the same examination. The signal intensity of each targeted SLN was measured three times, which were then averaged to reduce the measurement deviation of each SLN. All data were represented as mean ±standard deviation (SD) and normalized as percentage of change in signal intensity. The time-dependent signal profiles between two groups of mice were compared. The statistically significant differences between the group receiving free NIR830 and the group receiving IONP-NIR830 conjugates were assessed using the student's *t*-test. A *p*-value of less than 0.05 was taken to indicate statistical significance.

## Results

### MRI and NIR imaging properties of IONP-NIR830

NIR830 was successfully conjugated onto IONPs as confirmed by the absorption peak at 810nm in the optical spectrum shown in Figure 3(a), which presents the shift of the characteristic 790nm absorption peak of the free dye. The successful conjugation of NIR830 to IONPs is further supported by the control experiment in which neglectable NIR signal intensity from NIR830 was observed in the absorption spectrum of purified sample of IONPs without $-NH_2$ groups activated, after reacted with NIR830. The conjugation of NIR830 to IONPs did not significantly change the core size of IONPs. The overall

hydrodynamic size of IONP-NIR830 was 24nm with ξ potential of +2.1mV as measured in DLS experiments. Comparison between spectra of IONP-NIR830 and free NIR830, a red shift (~20 nm) of the absorption peak is observed, possibly due to the formation of J-aggregates.[27] The absorption spectrum also reveals that an increased shoulder peak at a lower wavelength 740 nm, which is also shifted from 720nm in its free form. Since this peak is considered to be attributed to the formation of dye aggregates,[26] in the case of nanoconstruct IONP-NIR830, the increase of the shoulder peak may be due to the conjugation of a relatively high concentration of dye molecules on the IONP surface. Based on the calibration curve obtained from free NIR830, it is estimated that the final dye concentration is 128 μM in concentrated solution with 1.0 mg/mL Fe. Based on the concentration of IONP, we calculated that there are ~320 NIR830 per particle. The optical imaging was applied to test the solution with IONP-NIR830 in both deionized water and phosphate buffered saline (PBS) with a series of dilutions. The emission intensity of IONP-NIR830 was concentration-dependent and still visible even at 1.28 μM of NIR830 and 0.05mM of Fe as shown in Figure 3(c). The transverse $T_2$ relaxation times of the IONP-NIR830 at different concentrations showed the strong $T_2$ shortening effect of the IONP-NIR830. Based on the concentration-dependent changes of $1/T_2$ as shown in Figure 3(b), the $r_2$ relaxivity of IONP-NIR830 was calculated as 166 $s^{-1}{\cdot}mM^{-1}$ at the field strength of 3 Tesla, similar to the IONP without NIR830 attached.

## NIR imaging of mouse SLNs

Both NIR830 and IONP-NIR830 conjugates were well tolerated by all mice used in the study. No local or systemic side effects were observed. In vivo imaging, the subcutaneous administration of both free NIR and MRI-NIR tracers into the middle phalange of the one fore footpad and into the middle digit of the one hind footpad resulted in a rapid delineation of the sentinel nodes (axillary and popliteal nodes) as early as 5 min after injection. Comparison of NIR images from mice before (Figure 4(a)) and after injection of free NIR830 (Figure 4(b)) and IONP-NIR830 (Figure 4(c)) allow the identification of lymph nodes. Each lymph node appeared as an oval-shaped structure as shown in Figure 4(b) and (c). As demonstrated on the images of one lower extremity, the sub-branch external iliac node was also seen at the site of near midline of the body (Figure 4(c)). In addition, the drainage lymphatic vessels were visualized in all mice that received tracers as shown in Figure 4(c).

Figure 5(a) shows a set of postcontrast optical images obtained at different times after administration of IONP-NIR830 conjugates, respectively. The IONP-NIR830 probe enabled visualization of SLN by NIR imaging with a fairly wide time window and the signal intensities of SLN changed gradually over the time as the tracers cleared from the nodes. It is noticed that the NIR signals increased in the abdominal regions in the later time points, suggesting that IONP-NIR830 nano-constructs were slowly accumulated in the liver after draining out from the lymph nodes. Figure 5(b) plots time-dependent changes of averaged NIR signal intensity in the SLN ($N$=6) after the administration of different imaging probes. Both free NIR-830 and IONP-NIR830 conjugates exhibited a signal increase from 5 to 15 min and peaks around 5–15 min in the auxiliary nodes after the injection. However, the interstitial administration of IONP-NIR830 led to a persistently plateau-like phase of peak

enhancement in the lymph nodes lasting 60 min after injection, whereas free NIR830 showed a gradual decline of signals in the lymph nodes 15 min after injection. Therefore, the IONP-NIR830 conjugate has a significantly longer time window of peak enhancement in the lymph nodes compared to that of NIR830 ($p<0.05$), suggesting that the lymphographic effect of IONP-NIR830 conjugates is superior to that of free NIR830. Compared with the time of sub-lymph nodes appearance, the time of sub-lymph nodes appearance in NIR830 group was significantly earlier (8.70±0.91 min) than those in IONP-NIR830 group (32.57±3.29 min, $p<0.05$; Table 1).

### MRI of SLN

The MR images using $T_2$ weighted fast spin echo and FLASH sequences reveal sentinel nodes that have taken up the IONP-NIR830 construct. Lymph nodes visualized on the NIR image (Figure 6(a)) exhibited signal drops in the $T_2$ weight MR images (Figure 6(b) and (c)) of the same animal. Comparing to the contra-lateral side where no IONP-NIR830 conjugates was administered, there is a significant drop in signal intensity at the areas of axillary and popliteal nodes, which showed high NIR signal in optical imaging. The MRI contrast with such signal void is typical $T_2$ weighted contrast effect from magnetic nanoparticles accumulated in the tissue. There is also 'bloom' effect (indicated in arrow) from the susceptibility artifact that is related to the local field inhomogeneity caused by magnetic nanoparticles at a high concentration. The areas of contrast change in SLN observed in MRI appear to be smaller than those observed in NIR images. The difference is mainly attributed to that MR images were obtained in the single slice (1mm thick), while NIR images are the projection across the thickness of the imaging object.

### Histological confirmation of image-indicated SLN

The presence of IONP-NIR830 conjugates in the SLN was further confirmed histologically by tracing the injected Evans blue dye and Prussian blue staining of nodes with IONP-NIR830. Lymph nodes exhibiting intense NIR signal in the NIR image (Figure 7(a)) were also visualized on the Evans blue image (Figure 7(b)). The blue-stained nodes appeared in the same areas as the nodes showed on NIR images. Prussian blue staining of the lymph nodes collected after the imaging experiments showed the presence of the Fe in the tissue sections (Figure 7(c)).

## Discussion

The availability of lymphotropic MR-NIR dual-contrast agent reported in the current study creates new possibilities for lymphography and SLN detection and biopsy. Compared to conventional SLN mapping with blue dye or radiotracer, integration of optical imaging and MRI methods in one setting is appealing given the complementary strengths from the high soft-tissue contrast and spatial resolution of MRI and the high sensitivity and real-time data acquisition of optical imaging.[28,29] MRI–optical imaging probes may facilitate preoperative identification of SLN metastases.[19] Several studies[18,19] have shown that Gd-based dual modality MRI and fluorescence imaging probe can be a useful agent for SLN mapping. However, there is a potential risk of Gd leaching from interstitially injected macromolecules with the potential for side effects and unknown toxic events.[30,31] On the other hand, in the

clinical practice of SLN mapping, fast clearance of small molecule SLN tracers, such as dyes, allows limited time window for survey of multiple SLN systemically. The time of detection from tracer injection and the duration of marking are important for the detection of SLNs in practical surgery. It is ideal that the tracer reaches SLNs soon after injection and is trapped for a long time without moving to another lymph node.[32]

Early studies have shown the feasibility of in vivo real-time multimodal or multicolor lymphatic imaging using different quantum dots with distinct visible-range emissions, which enabled simultaneous, but separate observation of multiple lymphatic basins in real-time.[33,34] The new dual modality MRI and NIR imaging probe developed in this study bridges two distinctive but complementary imaging modalities for SLN mapping. In this case, MRI can provide 3D visualization of tissue at high spatial resolution appropriate for presurgical planning, while optical imaging provides real-time intraoperative imaging. In the future development of this dual imaging probe, it is possible to conjugate multiple NIR molecules with emission wavelength at different ranges on the INOPs for mapping different lymphatic basins.

The dual imaging IONP-NIR830 probe reported here uses biodegradable INOPs. The fate and toxicity of INOPs have been investigated in the applications of lymph node imaging.[35] Interstitial IONP-NIR830 probes eventually accumulate in the liver and spleen hours after completion of SLN mapping as seen in our experimental results. It is presumable that INOPs could then be degraded and metabolized as reported.[36] In the current study, NIR830 developed in our laboratory was used for optical imaging. Since several FDA-approved optical dyes, such as indocyanine green (ICG), has been used for optical imaging applications in patients, the conjugation of FDA-approved ICG with IONPs could potentially provide an alternative dual MRI–optical probe for rapid translation of this MRI–optical imaging SLN mapping approach to the clinical applications. Importantly, the IONP-NIR830 probe (10nm core size) reported here has much longer lymph node retention time with a plateau of peak enhancement time lasting more than 60 min comparing to approximately 15 min when administering free NIR830. Our results (Table 1) showed that IONP-NIR830 conjugates took much longer time (>33 min) to reach the second echelon node compared with NIR830. Therefore, IONP-NIR830 nanoparticles are small enough to rapidly enter into lymphatic channels but are large enough to be trapped in lymph nodes. Furthermore, IONP-NIR830 nanoparticles are more suitable for accurate and reliable mapping SLNs in most surgical procedures, providing adequate time window for preoprative and intraoperative SLN mapping with MRI and optical imaging.

Interestingly, the current interstitial lymphography experiments using free NIR830 and bifunctional IONP-NIR830 tracer not only enables visualizing the SLNs draining from the injection sites in mice footpad, but also observing the external iliac lymph nodes which are considered as the second lymph nodes in the mice inguinal chain.

Although INOPs are used typically as signal voiding $T_2$ contrast agent that is not ideal for directly visualizing the afferent and efferent lymphatic vessels, previous studies by dynamic MRI using USPIO or ultrasmall iron oxide particles have shown that it is a useful technique for the detection of SLNs,[14,37] which SLNs were classified as the first lymph node(s) to

show susceptibility artifacts. Recently, it has been recognized that positive contrast was obtained by using ultrashort TE imaging from magnetic nanoparticles with different core sizes and concentrations.[38] Thus, it is potentially possible that MR lymphography for SLN mapping might rely on visualization of an afferent lymphatic coursing into a lymph node following interstitial injection of IONP. Meanwhile, compared to other fluorescent $T_2$-negative magnetic nanoparticles, such as fluorescent silica nanoparticles,[39,40] the NIR imaging capability from NIR830 dye provides IONP-NIR830 a higher signal-to-background ratio and better tissue penetration for detecting SLNs in combination of 3D deep tissue imaging capability of MRI that can be done preoperatively.

Previously, a number of reports have shown that bifunctional INOPs can be used for MRI as well as the optical imaging of brain tumor.[41] However, to our knowledge, the bifunctional magnetic fluorescent nanoparticles as a single molecule have rarely been applied in SLN identification prior to this study.

## Conclusions

A new class of MRI-NIR dual imaging tracer, IONP-NIR830 nanoparticle probe, has been developed for SLN mapping using magnetic INOPs conjugated with a NIR dye. IONP-NIR830 conjugates exhibit a longer plateau-like phase of peak-enhancement window and significantly longer lymph node retention time comparing to the small molecule dyes used in the conventional SLN mapping, proving a sufficient operating window for SLN mapping procedure which is crucial for reliable and accurate identification of SLNs.

In addition, this new probe is capable of not only mapping SLN but also tracing auxiliary lymph nodes. Therefore, reported dual-modal MRI–NIR imaging tracer offers good tissue penetration and sensitive detection of SLN. It can be applied for preoperative survey of lymph nodes with MRI and intraoperative SLN mapping using NIR optical devices.

## Acknowledgments

**Funding**

This work in parts is supported by grants from National Institutes of Health (NIH), Center of Cancer Nanotechnology Excellence (CCNE, U54 CA119338-01), in vivo Cellular and Molecular Imaging Center (ICMIC, P50CA128301-01A10003), Talent Summit Plan of Jiangsu Province (2009078), Science and Technology Development Plan of Nanjing (200905005) and Nanjing Medical Science and Technology Research Project (ZKX08019).

## References

1. Radovanovic Z, Golubovic A, Plzak A, et al. Blue dye versus combined blue dye-radioactive tracer technique in detection of sentinel lymph node in breast cancer. Eur J Surg Oncol. 2004; 30(9):913–917. [PubMed: 15498633]
2. Veronesi U, Galimberti V, Zurrida S, et al. Sentinel lymph node biopsy as an indicator for axillary dissection in early breast cancer. Eur J Cancer. 2001; 37(4):454–458. [PubMed: 11267853]
3. Aikou T, Kitagawa Y, Kitajima M, et al. Sentinel lymph node mapping with GI cancer. Cancer Metastasis Rev. 2006; 25(2):269–277. [PubMed: 16770539]
4. Frumovitz M, Ramirez PT, Levenback CF. Lymphatic mapping and sentinel lymph node detection in women with cervical cancer. Gynecol Oncol. 2008; 110(3 Suppl 2):S17–S20. [PubMed: 18502488]

5. Roberts AA, Cochran AJ. Pathologic analysis of sentinel lymph nodes in melanoma patients: current and future trends. J Surg Oncol. 2004; 85(3):152–161. [PubMed: 14991887]
6. Kaleya RN, Heckman JT, Most M, et al. Lymphatic mapping and sentinel node biopsy: a surgical perspective. Semin Nucl Med. 2005; 35(2):129–134. [PubMed: 15765375]
7. Sakorafas GH, Peros G. Sentinel lymph node biopsy in breast cancer: what a physician should know, a decade after its introduction in clinical practice. Eur J Cancer Care (Engl). 2007; 16(4):318–321. [PubMed: 17587354]
8. Marchal F, Rauch P, Morel O, et al. Results of preoperative lymphoscintigraphy for breast cancer are predictive of identification of axillary sentinel lymph nodes. World J Surg. 2006; 30(1):55–62. [PubMed: 16369717]
9. Choi SH, Kono Y, Corbeil J, et al. Model to quantify lymph node enhancement on indirect sonographic lymphography. AJR Am J Roentgenol. 2004; 183(2):513–517. [PubMed: 15269049]
10. Kobayashi H, Kawamoto S, Bernardo M, et al. Delivery of gadolinium-labeled nanoparticles to the sentinel lymph node: comparison of the sentinel node visualization and estimations of intra-nodal gadolinium concentration by the magnetic resonance imaging. J Control Release. 2006; 111(3): 343–351. [PubMed: 16490277]
11. Suga K, Yamamoto S, Tangoku A, et al. Breast sentinel lymph node navigation with three-dimensional interstitial multidetector-row computed tomographic lymphography. Invest Radiol. 2005; 40(6):336–342. [PubMed: 15905719]
12. Torchia MG, Nason R, Danzinger R, et al. Interstitial MR lymphangiography for the detection of sentinel lymph nodes. J Surg Oncol. 2001; 78(3):151–156. (discussion 157). [PubMed: 11745796]
13. Zhang C, Wang S, Xiao J, et al. Sentinel lymph node mapping by a near-infrared fluorescent heptamethine dye. Biomaterials. 2010; 31(7):1911–1917. [PubMed: 19963270]
14. Rasmussen JC, Tan IC, Marshall MV, et al. Lymphatic imaging in humans with near-infrared fluorescence. Curr Opin Biotechnol. 2009; 20(1):74–82. [PubMed: 19233639]
15. Soltesz EG, Kim S, Kim SW, et al. Sentinel lymph node mapping of the gastrointestinal tract by using invisible light. Ann Surg Oncol. 2006; 13(3):386–396. [PubMed: 16485157]
16. Kobayashi H, Kawamoto S, Star RA, et al. Micro-magnetic resonance lymphangiography in mice using a novel dendrimer-based magnetic resonance imaging contrast agent. Cancer Res. 2003; 63(2):271–276. [PubMed: 12543772]
17. Herborn CU, Vogt FM, Lauenstein TC, et al. Assessment of normal, inflammatory, and tumor-bearing lymph nodes with contrast-enhanced interstitial magnetic resonance lymphography: preliminary results in rabbits. J Magn Reson Imaging. 2003; 18(3):328–335. [PubMed: 12938128]
18. Koyama Y, Talanov VS, Bernardo M, et al. A dendrimer-based nanosized contrast agent dual-labeled for magnetic resonance and optical fluorescence imaging to localize the sentinel lymph node in mice. J Magn Reson Imaging. 2007; 25(4):866–871. [PubMed: 17345640]
19. Melancon MP, Wang Y, Wen X, et al. Development of a macromolecular dual-modality MR-optical imaging for sentinel lymph node mapping. Invest Radiol. 2007; 42(8):569–578. [PubMed: 17620940]
20. Talanov VS, Regino CA, Kobayashi H, et al. Dendrimer-based nanoprobe for dual modality magnetic resonance and fluorescence imaging. Nano Lett. 2006; 6(7):1459–1463. [PubMed: 16834429]
21. Strekowski L, Mason CJ, Lee H, et al. Synthesis of water-soluble near-infrared cyanine dyes functionalized with [(succinimido)oxy]carbonyl group. J Heterocyclic Chem. 2003; 40(5):913–916.
22. Yang L, Mao H, Wang YA, et al. Single chain epidermal growth factor receptor antibody conjugated nanoparticles for in vivo tumor targeting and imaging. Small. 2009; 5(2):235–243. [PubMed: 19089838]
23. Chen H, Wang L, Yeh J, et al. Reducing non-specific binding and uptake of nanoparticles and improving cell targeting with an antifouling PEO-b-Pgamma MPS copolymer coating. Biomaterials. 2010; 31(20):5397–5407. [PubMed: 20398933]
24. Chen H, Wu X, Duan H, et al. Biocompatible polysiloxane-containing diblock copolymer PEO-b-Pgamma MPS for coating magnetic nanoparticles. ACS Appl Mater Interfaces. 2009; 1(10):2134–2140. [PubMed: 20161520]

25. Atkins RC. Colorimetric determination of iron in vitamin supplement tablets. A general chemistry experiment. J Chem Educ. 1975; 52(8):550. [PubMed: 1165254]
26. Duan HW, Kuang M, Wang XX, et al. Reexamining the effects of particle size and surface chemistry on the magnetic properties of iron oxide nanocrystals: new insights into spin disorder and proton relaxivity. J Phys Chem C. 2008; 112(22):8127–8131.
27. Nasr C, Liu D, Hotchandani S, et al. Dye-capped semiconductor nanoclusters. Excited state and photosensitization aspects of rhodamine 6G H-aggregates bound to SiO2 and SnO2 colloids. J Phys Chem-Us. 1996; 100(26):11054–11061.
28. Frullano L, Meade TJ. Multimodal MRI contrast agents. J Biol Inorg Chem. 2007; 12(7):939–949. [PubMed: 17659368]
29. Jennings LE, Long NJ. 'Two is better than one' – probes for dual-modality molecular imaging. Chem Commun. 2009; 24:3511–3524.
30. Grobner T. Gadolinium – a specific trigger for the development of nephrogenic fibrosing dermopathy and nephrogenic systemic fibrosis? Nephrol Dial Transpl. 2006; 21(6):1745–1745.
31. Marckmann P, Skov L, Rossen K, et al. Nephrogenic systemic fibrosis: suspected causative role of gadodiamide used for contrast-enhanced magnetic resonance imaging. J Am Soc Nephrol. 2006; 17(9):2359–2362. [PubMed: 16885403]
32. Nakajima M, Takeda M, Kobayashi M, et al. Nanosized fluorescent particles as new tracers for sentinel node detection: experimental model for decision of appropriate size and wavelength. Cancer Sci. 2005; 96(6):353–356. [PubMed: 15958058]
33. Kosaka N, Ogawa M, Sato N, et al. In vivo real-time, multicolor, quantum dot lymphatic imaging. J Invest Dermatol. 2009; 129(12):2818–2822. [PubMed: 19536144]
34. Kobayashi H, Hama Y, Koyama Y, et al. Simultaneous multicolor imaging of five different lymphatic basins using quantum dots. Nano Lett. 2007; 7(6):1711–1716. [PubMed: 17530812]
35. Bourrinet P, Bengele HH, Bonnemain B, et al. Preclinical safety and pharmacokinetic profile of ferumoxtran-10, an ultrasmall superparamagnetic iron oxide magnetic resonance contrast agent. Investig Radiol. 2006; 41(3):313–324. [PubMed: 16481915]
36. Chouly C, Pouliquen D, Lucet I, et al. Development of superparamagnetic nanoparticles for MRI: effect of particle size, charge and surface nature on biodistribution. J Microencapsul. 1996; 13(3): 245–255. [PubMed: 8860681]
37. Rogers JM, Jung CW, Lewis J, et al. Use of USPIO-induced magnetic susceptibility artifacts to identity sentinel lymph nodes and lymphatic drainage patterns. I. Dependence of artifact size with subcutaneous Combidex (R) dose in rats. Magn Reson Imaging. 1998; 16(8):917–923. [PubMed: 9814774]
38. Zhang LJ, Zhong XD, Wang LY, et al. T(1)-eeighted ultrashort echo time method for positive contrast imaging of magnetic nanoparticles and cancer cells bound with the targeted nanoparticles. J Magn Reson Imaging. 2011; 33(1):194–202. [PubMed: 21182139]
39. Cong LM, Takeda M, Hamanaka Y, et al. Uniform silica coated fluorescent nanoparticles: synthetic method, improved light stability and application to visualize lymph network tracer. Plos One. 2010; 5(10):e13167. [PubMed: 20976187]
40. Jeon YH, Kim YH, Choi K, et al. In vivo imaging of sentinel nodes using fluorescent silica nanoparticles in living mice. Mol Imag Biol. 2010; 12(2):155–162.
41. Kircher MF, Mahmood U, King RS, et al. A multimodal nanoparticle for preoperative magnetic resonance imaging and intraoperative optical brain tumor delineation. Cancer Res. 2003; 63(23): 8122–8125. [PubMed: 14678964]

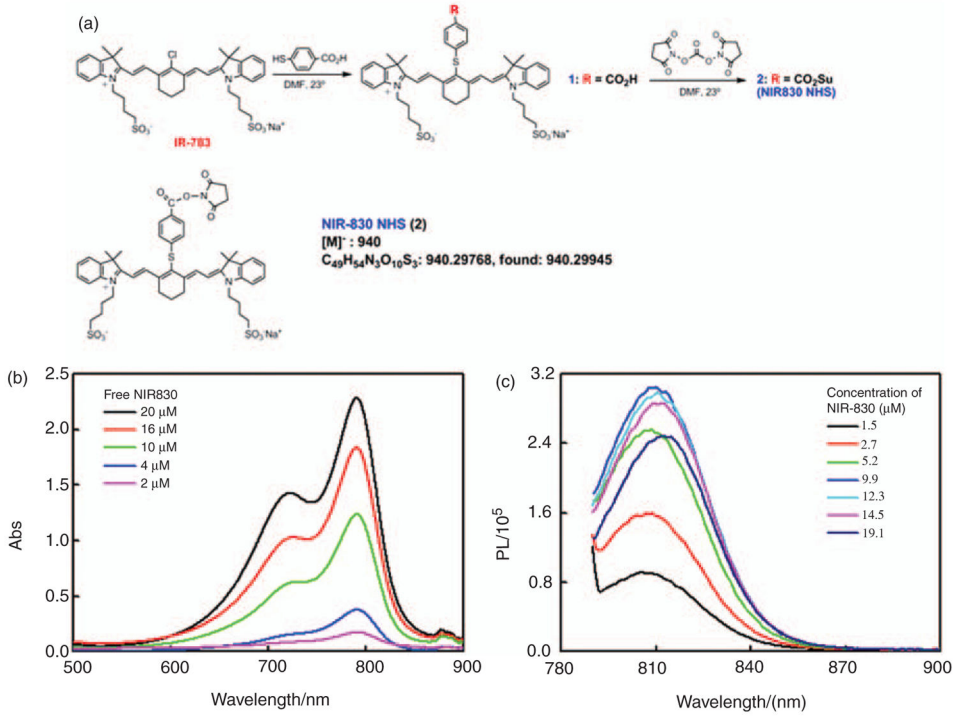


**Figure 1.**

The synthetic scheme and structure of NIR830-NHS (a). An absorption spectrum (b) and a fluorescence spectrum (c) of NIR830-NHS at different concentrations in the water solvent are shown.

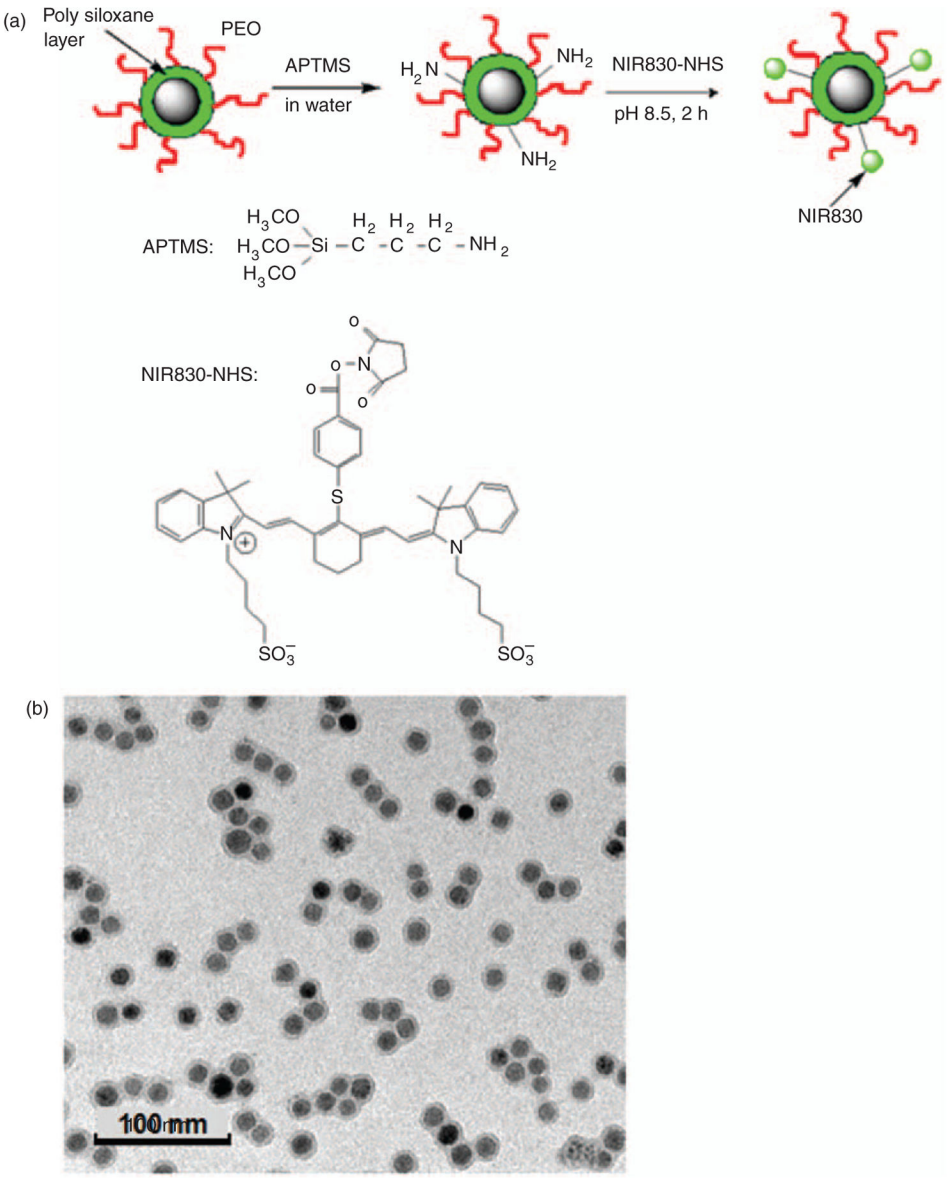


**Figure 2.**

The scheme for conjugation of NIR830 to IONPs (a). The image of transmission electron microscopy (TEM) shows the well dispersed single core iron oxide nanoparticles (IONPs) with an averaged core size of 10 nm (b). The averaged core size was obtained from measuring the diameters of 50 nanoparticles in the field of view.

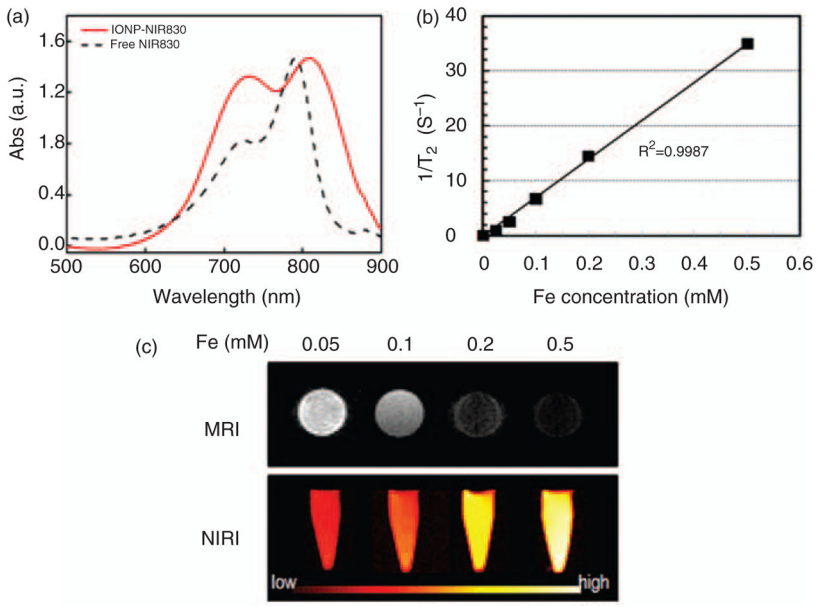


**Figure 3.**

Conjugation of NIR830 to iron oxide nanoparticles (IONPs) was confirmed by observing emission of NIR830 peak at 830 nm in the spectrum of IONP-NIR830 (a). The transverse $T_2$ relaxation times of the IONP-NIR830 are iron concentration-dependent (b), allowing for calculating the $r_2$ relaxivity of IONP-NIR830 (~166 $s^{-1}mM^{-1}$ at 3T). Signal intensities of near infrared (NIR) image and $T_2$ weighted images of IONP-NIR830 at different iron (Fe) concentrations (c).

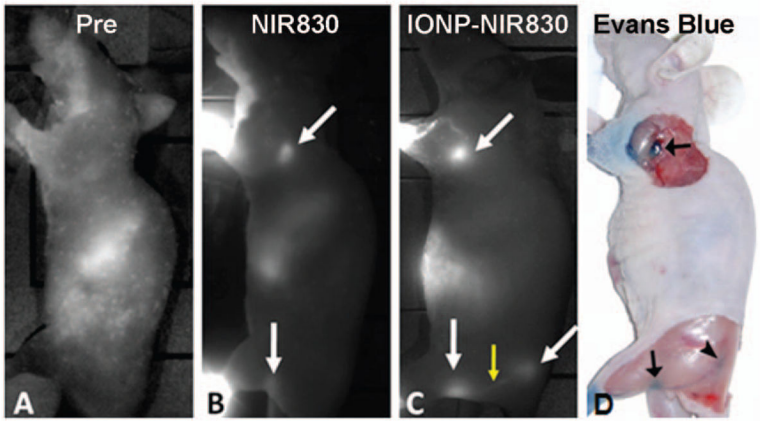


**Figure 4.**

Near infrared (NIR) images of the animals before (a) and after received NIR830 (b) and IONP-830 (c) sentinel lymph node (SLN) tracing agents. Lymph nodes with increases of NIR signal intensities were indicated in arrows (white). The increased NIR signals can be seen in the lymph node drainage as indicated by the yellow arrow. SLNs visualized from NIR images were also identified after injection of Evans blue dye at the same site of the same animal (d). Images were selected from those collected 90 min after the injection. The lower signal intensity at the lymph nodes in the animal receiving NIR830 is due to faster clearance of the free small NIR dye comparing to that of high molecular weight of the IONP-NIR830 nanoconstruct.

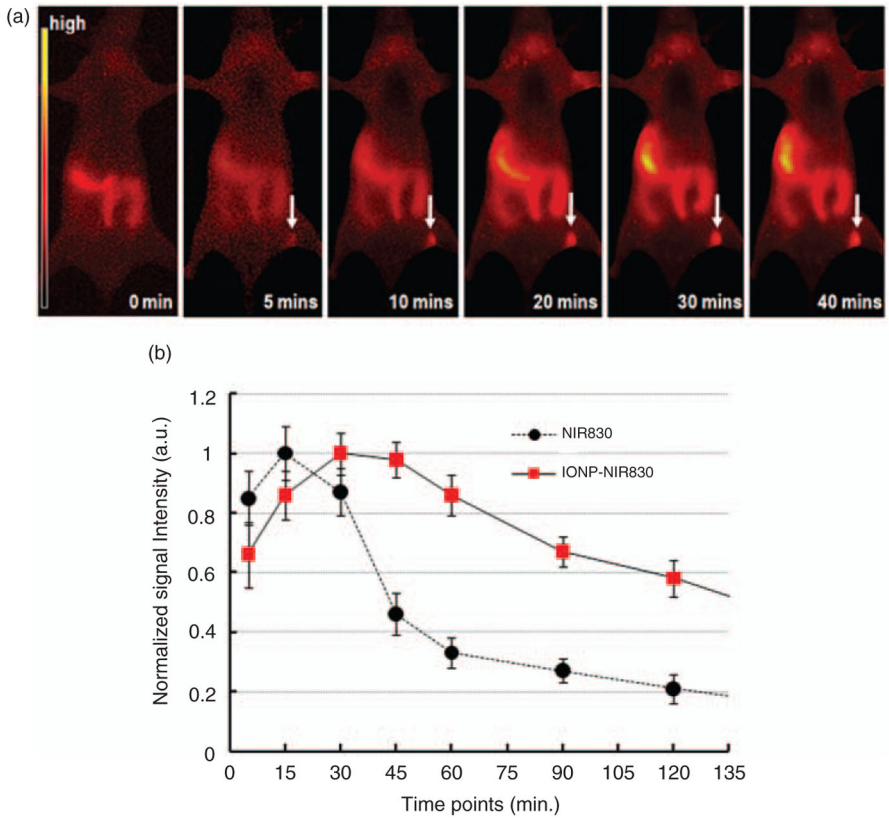


**Figure 5.**

Near infrared (NIR) images at different time points before and after administered IONP-NIR830 (a) and signal intensity profiles in sentinel lymph nodes (SLNs) tracked by either free NIR830 or IONP-NIR830 (b). Data at each time point were averaged from those collected from six animals. The signal intensities arbitrary unit (a.u.) were normalized based on the highest signals for both groups. The absolute signal intensity of free NIR dye (3800 a.u.) was approximately twice higher than that of IONP-NIR830 (2010 a.u.). Reduction of the NIR signal intensity in IONP-NIR830 is due to the quench effect from the aggregation of NIR830 dyes on the iron oxide nanoparticles (IONP) surface. It is noticed that increased signal intensity in the right abdominal area is likely due to the accumulation of IONP-NIR830 nanoparticles in the liver after cleared out of the lymph nodes via lymphatic drainage.

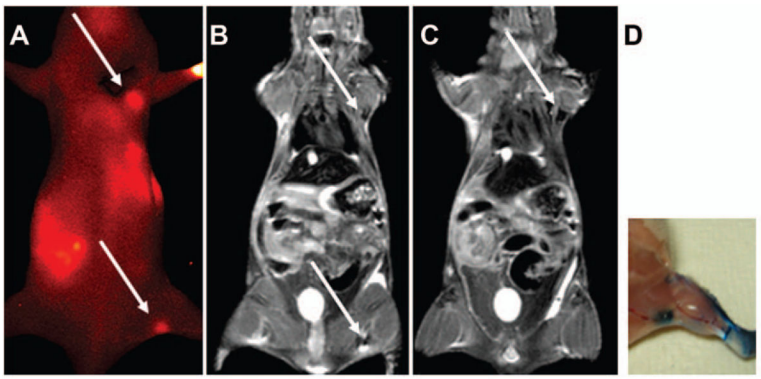


**Figure 6.**

An example of sentinel lymph nodes (SLNs) in a mouse detected by near infrared (NIR) (a) and magnetic resonance imaging (MRI) (b and c) after being injected with IONP-NIR830. Arrows indicate the lymph nodes seen in MR or NIR images. Notice that MR images selected have thin slice thickness (1 mm), while the NIR image is from the entire depth of the animal body. The locations of SLN identified from MRI and NIR imaging was confirmed by the conventional lymph node tracking method with Evens blue dye (d).

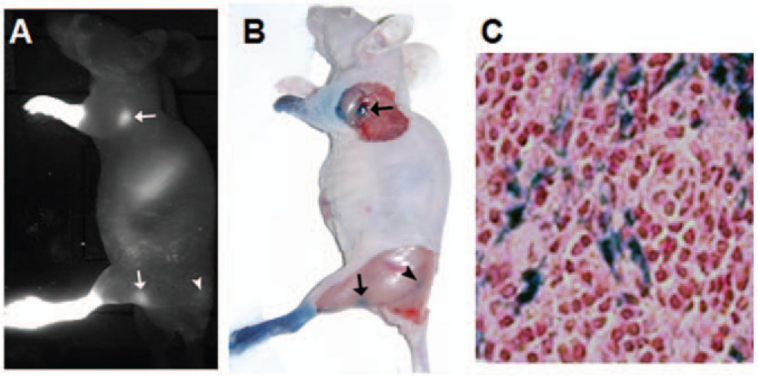


**Figure 7.**

Near infrared (NIR) optical imaging of the auxiliary lymph node as well as sentinel lymph node (SLN) using IONP-NIR830 (a), which is correlated well with the observations of Evens blue tracing of lymph nodes in the same mouse (b). The histological confirmation of the presence of iron oxide nanoparticles (IONP) in SLN was provided by the positive Prussian blue staining for iron in the section of the collected lymph nodes (c).

**Table 1**

Time of sublymph nodes appearance in two experimental groups measured on optical lymphographic images with NIR830 dye and IONP-NIR830.

| Tracer | Time (min)[a] |
|---|---|
| NIR830 dye | 8.70±0.91 |
| IONP-NIR830 | 32.57±3.29 |

[a]Values are mean±standard deviation, $n$=6; $p$<0.05, NIR830 dye versus IONP-NIR830.